The first order L-G phase transition in liquid Ag and Ag-Cu alloys is driven by deviatoric strain

Qi An^{1*}, William L. Johnson^{2*}, Konrad Samwer³, Sydney L. Corona², and William A. Goddard III^{4*}

¹Department of Chemical and Materials Engineering, University of Nevada-Reno, Reno, Nevada

89557, USA

²Keck Engineering Laboratories, California Institute of Technology, Pasadena, CA 91125, USA

³I. Physikalisches Institut, University of Goettingen, 37077 Goettingen, Germany

⁴Materials and Process Simulation Center, California Institute of Technology, Pasadena, CA 91125, USA.

*Correspondences: qia@unr.edu; wlj@caltech.edu; wag@caltech.edu

Abstract: An undercooled liquid-phase (L-phase) can undergo a first order configurational phase transition to either a crystal phase (X-phase) or a metastable, configurationally heterogeneous, rigid glassy phase (G-phase). To investigate the underlying mechanism of the L-G transition, we employ molecular dynamics simulations to study G-phase formation in a binary Cu-Ag system. We find that G-phase formation is driven by the reduction of local distortion energy arising from deviatoric strains in the liquid phase and demonstrate its local distribution. Reduction of distortion energy contributes over 80% of the latent heat of the L-G transition, suggesting that condensation of spatially varying random elastic fields in the liquid is primarily responsible for the first order L-G transition. By applying this analysis to crystallization and G-phase formation in elementary Ag, we show that deviatoric strain

Key words: Metallic glasses, Glass transition, MD-simulation, Embedded Atom Model, Elasticity

energy is the dominant driving force for the L-G and L-X transition also in the case of the pure metal.

1

The existence of liquid-liquid phase transitions has been reported in numerous studies of molecular liquids, liquid semiconductors, and metallic liquids [1-9]. In two recent publications [10,11], we demonstrated that both deeply undercooled liquid Ag and binary eutectic Ag-Cu alloys undergo a first order phase transition from a disordered homogeneous liquid L-phase to a metastable heterogeneous intermediate phase, designated as the G-phase. While the G-phase possesses local regions that exhibit crystalline-like short range order, long range order is absent. As such, the G-phase was identified as glassy. The ordered regions are spatially isolated, mutually uncorrelated, and separated by a continuous network of disordered liquid-like regions. The two regions are spatially inter-mixed displaying a characteristic heterogeneity length scale Λ ranging from ~1 nm in Ag-Cu eutectic alloys to 4~5 nm for the pure Ag (or Cu). The G-phase might aptly be described as a nanoscale "mixed state" or a nano-scale composite. It is a metastable state of matter that ultimately crystallizes. However, the lifetime of this characteristic heterogeneous structure far exceeds the configurational relaxation time by many orders of magnitude thereby justifying describing the G-phase as a metastable phase. Upon reheating, the G-phase was observed to reversibly transform back to the Lphase without intervening crystallization. The G to L melting transition is first order, displaying latent heat and hysteresis. The transition occurs at a well-defined L-G coexistence temperature lying well below the melting point of the competing crystalline phase (phases for the alloy case). Reversibility demonstrates the L-G transition is in fact a discontinuous equilibrium phase transition between two metastable phases. The L-G transition was very recently proposed to explain metallic glacial glass (MGG) formation in a rare-earth-element-based bulk metallic-glass compositions, where the product MGG-phase displays first order melting upon heating and shows a relatively large increase in hardness by 20% compared with as quenched L-glass [12]. In other recent work on ultra-fragile Pt-Cu-P bulk glass forming liquids [13], some authors reported that the glass transition itself evolves into a first order melting transition in the high fragility limit of liquids. This suggests a more fundamental connection between the L-G transition and glass formation.

Liquid metals and alloys become rigid on cooling either by crystallizing or by glass formation. Crystallization is a first order thermodynamic phase transition wherein long range atomic translational symmetry emerges in the product solid phase. A glass may exhibit short range atomic order, but lacks such long range translational symmetry. A glass is distinguished from a liquid by its lack of fluidity; glasses are kinetically frozen and exhibit mechanical rigidity on practical time scales. Solidification may correspondingly be viewed either in terms of a change in symmetry or as emergence of elastic rigidity. While both equilibrium liquids and crystals support external pressure, a liquid does not resist shape changes. The liquid shear modulus vanishes ultimately on practical time scales. Glasses, by contrast, display mechanical rigidity and a finite shear modulus on relatively long time scales. The glass transition reflects a dramatic change of time scale over which shear rigidity is observed. A simple elemental metal crystal (e.g. fcc, bcc, etc.) with inversion symmetry is inherently free of internal deviatoric stress. Alexander [14], Vitek [15], among others [16], have used the virial expression to define atomic level stresses in liquids and glasses. For liquids, deviatoric atomic stresses are dynamic, fluctuate rapidly on the scale of atomic vibrational motion, but average to zero over time scales exceeding the configurational relaxation time of the liquid, typically in the ps time range. In a glass, atomic stresses are frozen and persist over much longer time scales giving rise to a non-vanishing, frozen-in, and spatially varying internal stress field. In the absence of applied external stress, the macroscopic ensemble average of this stress vanishes, but the microscopic deviatoric stress at a given location in the glass is finite. The kinetic glass transition is reflected by the dramatic increase in persistence time of the frozen internal stress field. This naturally leads to the question of how internal stresses evolve during the recently identified first order L-G transition [10,11].

From a thermodynamic perspective, the G-phase configurational enthalpy (i.e. potential energy (PE)) lies between that of the homogeneous liquid L-phase and the crystal X-phase in the undercooled region. At low temperature, the G-phase displays local ordered core regions of low enthalpy, making it energetically more stable than the liquid phase. The surrounding disordered liquid-like regions (shell) lead to a configurational enthalpy that lies above that of the crystal but below that of the L-phase. Upon fast heating, the G-phase melts into the L-phase owing a higher configuration entropy. In the present work, we investigate the contribution of atomic level stress to the configurational enthalpy and potential energy of the L- and G-phases. In particular, we investigate the spatial structure and temporal behavior of the deviatoric stress field during the transition for both phases. For the G-phase, we demonstrate that the frozen deviatoric contribution to the internal stress field has a spatial structure and correlation length Λ that corresponds with that of the heterogeneous G-phase structure. The Λ describes short range order of the G-phase as revealed by variations in bond orientational order on passing from ordered core regions to surrounding liquid-like shell regions. By comparison, deviatoric atomic stresses in the L-phase are greater in magnitude, spatially homogeneous, and rapidly fluctuating. By computing the total elastic strain energy associated with internal stresses, we demonstrate that the latent heat of the L-G transition is dominated by a reduction in deviatoric strain energy. Essentially, the transition can be viewed in terms of a condensation of the microscopic stress field in the L-phase to spatially ordered stress field of lower potential energy in the G-phase.

In previous studies [10,11], we suggested that the G-phase forms by nucleation from the L-phase. If this is the case, a description using classical nucleation theory would require defining an interface and an interfacial free energy between the two phases. Given the heterogeneity of the G-phase on Λ , the L-G interface cannot be atomically sharp, but rather must be defined on a scale greater than Λ . Therefore, to simulate G-phase nucleation using molecular dynamics (MD) requires an MD cell

size, L, at least several multiples of Λ to avoid finite size effects. This MD would enable one to identify the L-G interface and to define islands of G-phase growing at the expense of L-phase in the two-phase regime. To address this problem, we carried out large isothermal simulations of the L-G transition in Ag-Cu alloys with $\Lambda \sim 1-2$ nm on systems with a 38 nm x 38 nm x 3.8 nm periodic cell. This enabled identification of G-phase islands that form and grow at the expense of the L-phase in the two phase regime. Using such simulations, we characterized the L-G two-phase microstructure during the transformation. Several methods were employed to identify the G-phase regions. The two phases are distinguished by their differing short range order. As noted from previous studies [10,17], Honeycutt-Andersen analysis provides one method to fingerprint short range order. In the present work, we used orientational bond order parameters, q₈, to provide another means to distinguish atomic clusters belonging to regions of L- vs. G- short range order [18,19]. The microstructure revealed from this analysis was compared with that obtained by mapping spatial variation of PE per atom (PE mapping) as well as that obtained by spatial mapping of deviatoric strain energy per atom. Remarkably, the three methods reveal the same common underlying L-G microstructure. The results show that the L-G microstructure is equivalently described by mapping the spatial variation of either short range order, configurational enthalpy per atom, or deviatoric strain energy density. As a final step to determine if short range chemical ordering plays a role in the L-G transition for the alloy case, we assessed the number of nearest neighbor pairs of like atoms (Ag-Ag, Cu-Cu) and unlike atoms (Ag-Cu) in both phases. The results show the fractions of each pair type is essentially identical in the two phases. Atomic clustering of like atoms remains unchanged during the transformation. This demonstrates that the L-G transition is not related to chemical ordering, but rather to a topological reconstruction of the atomic bonding network resulting in an increase of rigidity.

The large-scale MD simulation were performed using lammps software [20] and Embedded Atom Model (EAM) potential [21]. The simulation details could be found in Supplementary Materials

(SM). The strain energy density consists volume change and distortion change [22]. The details of computing strain energy using Von-Mises stress [23,24], Voronoi volume [25] and elastic modulus [26] are in the SM. Figure S1 of SM indicated that the strain energy could be applied to characterize the long-range elastic energy around defects, as predicted from dislocation theory [27]. The details of computing bond-orientational order parameters [28,29] and PE-density map are also discussed in SM.

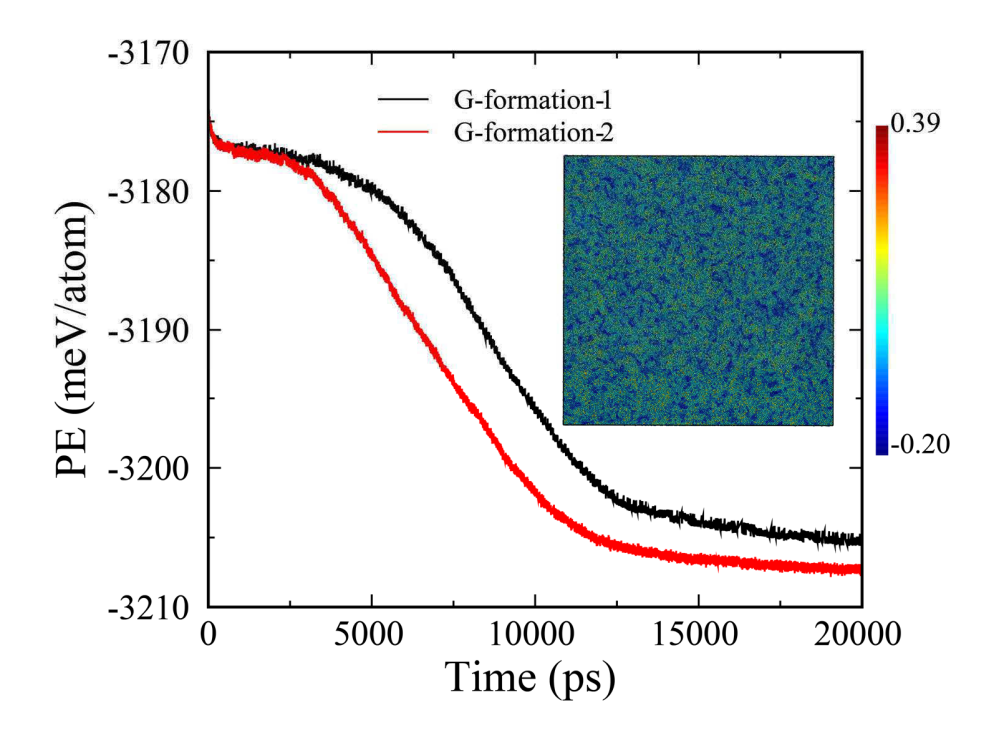


Figure 1. The L-G transition in the quasi-2D Cu-Ag system is indicated by the PE decrease within 20 ns for isothermal MD runs at 700 K. The insert is the G-phase formed in the first MD run, color coded by relative PE density map.

The first order L-G transition is characterized by the latent heat evolved as the L-phase transforms to G-phase. Figure 1 displays two independent isothermal MD runs of the L-G transition in Cu₇₅Ag₂₅ alloy at 700 K. The PE of L-phase reaches constant within the first 200~300 picoseconds after quenching from high temperature, indicating that the L-phase reaches equilibrium before the transition. After ~3 nanoseconds, the PE starts to drop, continuously dropping by ~28 meV/atom over a

timescale of ~10 ns, indicating the L-G transition. Thus, the latent heat of the L-G transition in this quasi-2D system is ~28 meV/atom, which is consistent with our previous study [10]. Additionally, the L-G transition completes over ~10 nanoseconds, much longer than either the L-G or L-X transition in elementary Ag [10,11]. The G-phase formed is displayed in Figure 1. It exhibits a heterogeneous composite structure that remains stable over 5 nanoseconds. Two independent MD runs leads to slightly different final PEs for G-phases because of the different transition process discussed below.

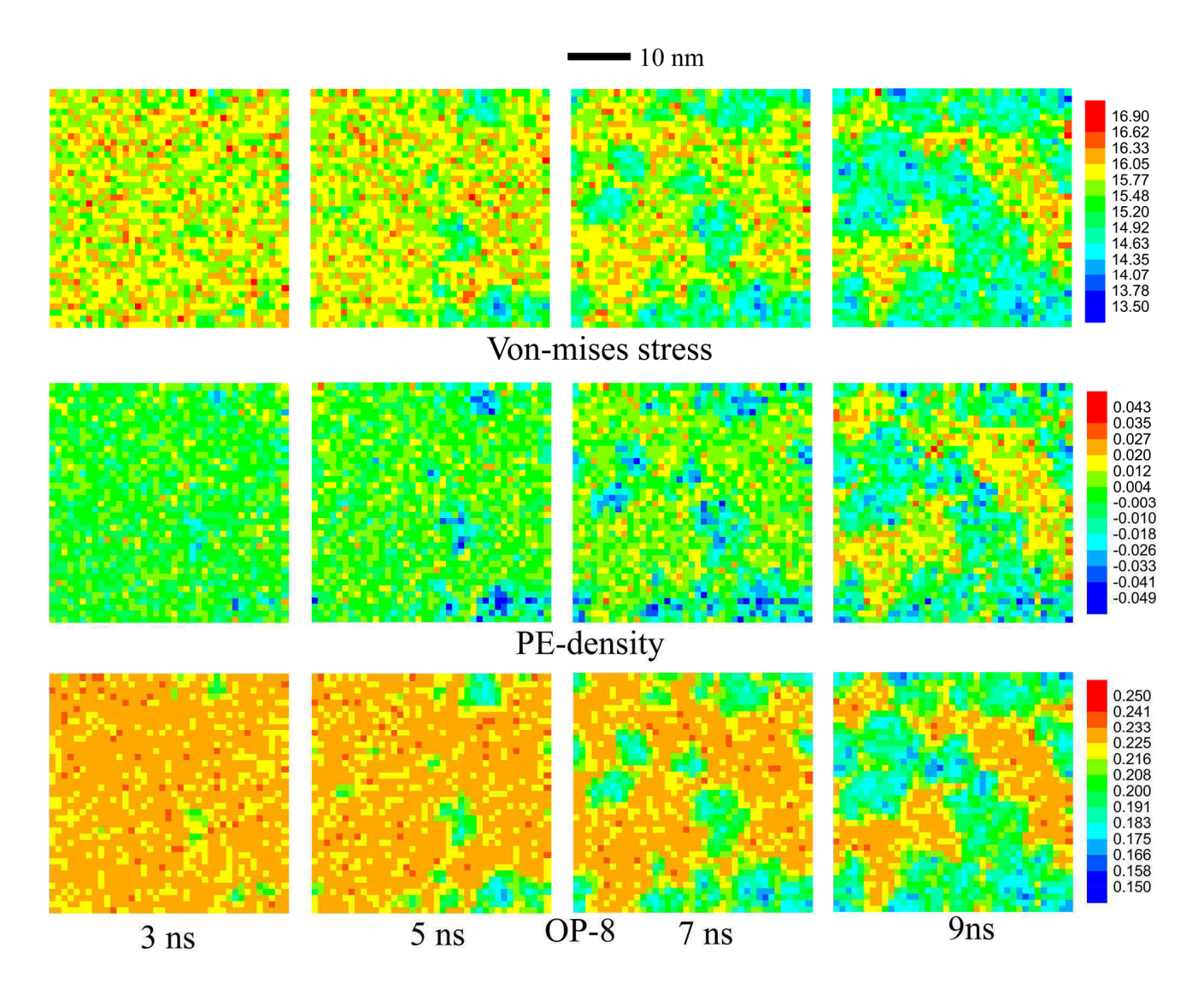


Figure 2. The L-G transition is characterized by the σ_v , PE-density, and bond-orientation order parameter (q₈) analyses. Several snapshots are displayed here. More details of q₈ and σ_v at various stages are in Figure S2 and S3 of SM, respectively.

The relative long period of the L-G transition in Cu₇₅Ag₂₅ compared to the L-G transition in Ag suggests that the thermodynamic driving force is relatively smaller in the alloy so that the L-G interface may not be sharp. To examine the microstructure evolution in the L-G transition, we performed analyses of q_8 , the PE-density, and the von-mises stress (σ_v) for each atom in the simulation cell. Then these physical properties were coarse-grained using 1 nm × 1 nm bins (~280 atoms) in the x-y plane to illustrate the microstructure evolution during the L-G transition. Figure 2 displays these coarse-grained physical properties showing several important snapshots during the L-G transition for the first MD run in Figure 1. As the L-G initially occurs at ~3 ns, we observes formation of several local G-phase droplets that have lower PE-density, reduced σ_v , and smaller op-8 compared to the surrounding Lphase. Then these droplets start to grow and merge. As shown in the 5 ns snapshot, two small droplets merge to a larger one at the lower right corner of the system. Meanwhile more G-phase regions are present as indicated by the smaller q_8 , lower PE-density, and reduced σ_v . As small droplets continuously grow and amalgamate, several large G-phase islands are present, as shown in the 7 ns snapshot, which corresponds to 1/3 of the L-G transition based on the PE curve in Figure 1. At 9 ns, these G-phase islands combine to one big G-phase that percolates along the whole simulation cell. This provides clear evidence that the op-8, the PE-density, and σ_v correlate very well in the G-phase formation process, suggesting that σ_v and PE-density correlate as the local ordered structure develops. A more detail evolution of q_8 and σ_v during the G-phase formation is shown in Figure S2 and Figure S3 of SM, respectively.

To illustrate the possible chemical effects on the L-G transition, we performed chemistry analysis on the L-G transition using the same coarse-grained approach and 1 nm × 1 nm bins. To represent the chemistry deviation from the composition Cu₇₅Ag₂₅, we assigned -0.25 to each Cu atom and +0.75 to each Ag atom so that the average composition Cu₇₅Ag₂₅ has a value of zero. A region above zero represents a Ag rich region while one below 0 represents the Cu rich region. As shown in Figure S4 in the SM, the chemistry *does not correlate* with the L-G transition although there is some spatial heterogeneity over the whole sample. Additionally, we assessed the number of nearest neighbor pairs of like atoms (Ag-Ag, Cu-Cu) and unlike atoms (Ag-Cu) in both phases. For the G-phase the ratios of Ag-Ag, Cu-Cu and Cu-Ag are 11.01%, 61.33%, and 27.66%, respectively. In comparison, these ratios in L-phase are 10.85%, 60.15% and 29.00% for Ag-Ag, Cu-Cu and Cu-Ag, respectively. Therefore, the neighbor pairs display little change over the L-G transition. These analyses suggest that the L-G transition is a topological rigidity transition with almost no relationship with chemistry.

We performed similar analyses of σ_v and q_8 for the second independent MD run of the L-G transition. The detailed evolution of σ_v and q_8 are displayed in Figure 3 and Figure S5 of the SI, respectively. The initial formation process is similar for the 2^{nd} run with a few droplets present in the process. Different from the 1^{st} L-G transition, the initial droplets in the 2^{nd} run are close to each other and merge to amalgamate faster in the early stage of growth to form one large G-phase droplet. This causes a faster growth rate in the initial G-phase growth for the 2^{nd} run. This is consistent with the PEcurves in Figure 1, showing that the slope of initial growth processes is sharper for the 2^{nd} run than the 1^{st} run. As this large G-phase droplet expands to the whole simulation cell, the L phase transforms completely to the G-phase. The metastable G-phase structures from both MD simulations display slightly different microstructures in which the local ordered regions in simulation 2 is larger than simulation 1, as shown by the 20-ns snapshot in Figure S2 and S5 of SM. The larger local order regions lead to a lower PE energy of G-phase in simulation 2, as displayed in Figure 1.

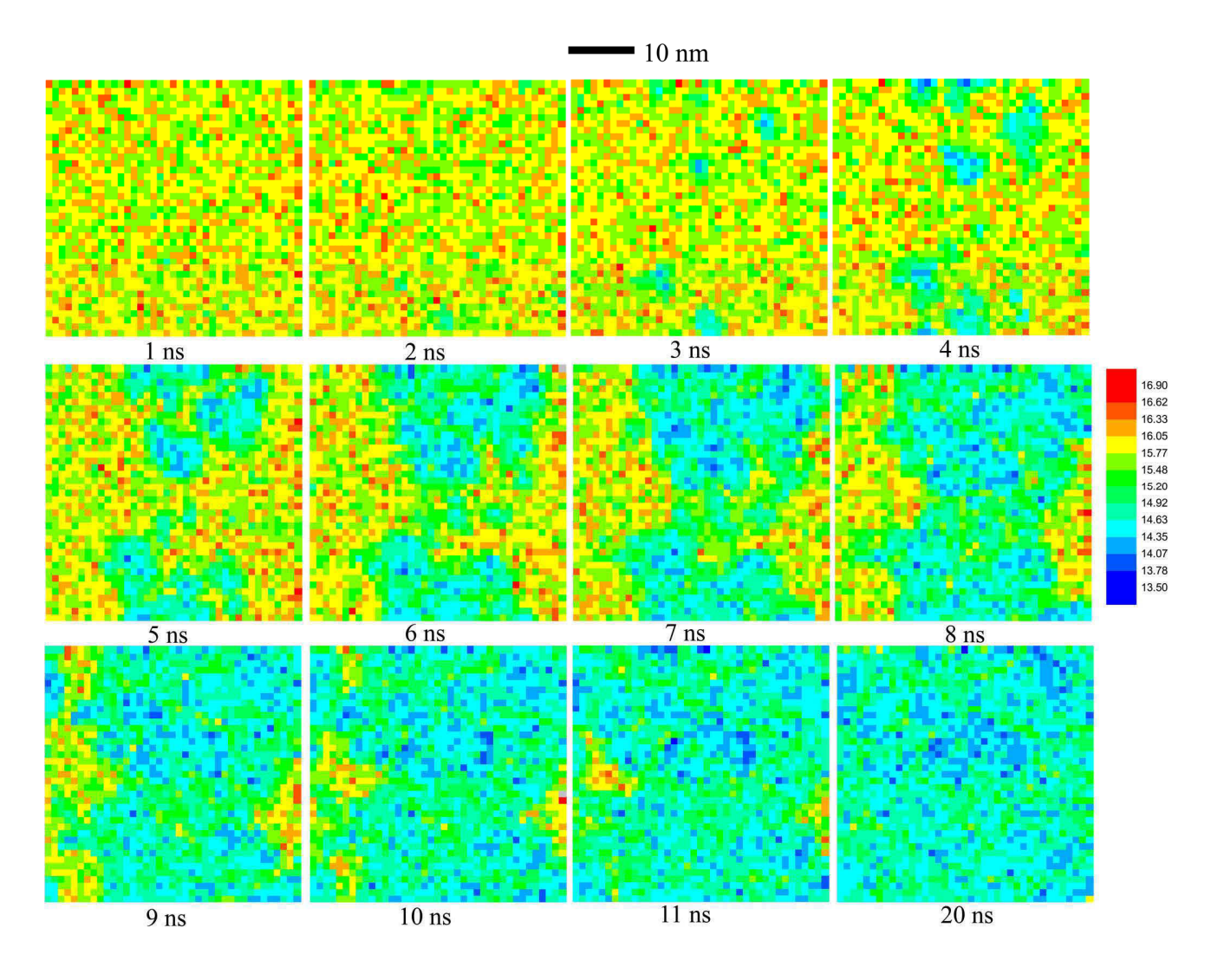


Figure 3. The detailed microstructure evolution of L-G transition characterized by von-mises stress. This is the second MD run corresponding to the red PE curve in Figure 1.

Our previous studies suggested that the reduction in enthalpy is the thermodynamic driving force for the first order L-G transition [10,11]. The microstructure evolution during L-G transition shows a good correlation between PE-density and σ_v , indicating that the condensation of the elastic field in the L-phase is the fundamental driving force for this first order L-G transition. To validate this idea, we computed the distortion energy of both L-phase and G-phase for the 1st MD run and compare it to the latent heat of the L-G transition. The average von-mises stress of the L-phase, σ_{v_L} , is 15.85 GPa per atom using the configuration at 1.0 ns (Figure 1). The Young's modulus E_L and Poisson ratio

 v_L of L-phase are 113.12 GPa and 0.45, respectively. The computed average atomic volume of L-phase, Ω_L , is 14.11 Å³. Thus, using equation S(1) of SM, the distortion energy density of L-phase, U_{s_L} , is calculated to be 94.6 meV per atom. Then we applied the same approach to the G-phase, leading to a distortion energy of G-phase, U_{s_L} , of 72.4 meV per atom, giving $\sigma_{v_L} = 14.72$ GPa, $E_G = 123.72$ GPa, $V_G = 0.42$, and $\Omega_L = 13.98$ Å³, respectively. Therefore, the reduction of distortion energy in the L-G transition is 22.2 meV, which can be compared to the latent heat of L-G transition of ~27.5 meV. This accounts for ~83% of the latent heat, suggesting that the reduction in deviatoric strain energy plays a dominate role in the first order L-G transition. We also computed the $\Delta(PV)$ term contribution to the latent heat and find that it accounts for only ~1% of latent heat. This is reasonable since our simulation is under constant pressure conditions, so that $\Delta(PV)$ is not expected to contribute significantly to the latent heat of L-G transition.

We also examined the deviatoric strain energy change during the L-G and L-X transition in elementary Ag, as discussed in the SM and Figure S6-S8. The simulation results indicated that the deviatoric strain energy is also the origin for the L-G and L-X transition. It is worth to notice that the von Mises stress field has the same heterogeneity length scale as PE, as shown in Figure S7 of SM. This further demonstrates that the reduction of distortion energy is the driving force for the L-G transition.

In summary, we carried out MD simulations to illustrate the fundamental driving force for the first order L-G transition in Cu₇₅Ag₂₅ and elementary Ag systems, as well as the L-X transition in Ag. The L-G microstructure in quasi-2D Cu₇₅AG₂₅ system is consistently revealed by mapping the spatial variation of short range order, configurational enthalpy per atom, or deviatoric strain energy density. But the short range chemical ordering is not correlated with the L-G transition for Cu₇₅Ag₂₅. Moreover, the reduction of distortion energy accounts for over 80% latent heat in L-G transition. Our simulations

indicate that the L-G transition is a topological reconstruction of the atomic bonding network driven by the reduction of distortion energy in L-phase. Furthermore, we performed the same analysis on crystallization and G-phase formation in elementary Ag and found that deviatoric strain energy is also the driving force for the L-G and L-X transition in pure Ag. We propose that the underlying mechanism of the first order L-G and L-X transitions in metallic liquids involves emergence of elastic rigidity by condensing the random elastic field in L-phase.

Acknowledgements

W.L.J and S.C. are supported by NSF grant with the award number DMR 1710744. K.S. is supported by the DFG, grant Sa337/10. W.A.G. I supported by ONR (N00014-19-1-2081).

Competing interests

The authors declare no competing interests.

References

- [1] O. Mishima, Y. Suzuki, Nature 419 (2002) 599–603.
- [2] M. Zhu, J. Q. Wang, J. H. Perepezko, L. Yu, J. Chem. Phys. 142 (2015) 244504.
- [3] L. Cohen, A. Ha, X. Zhao, M. Lee, T. Fischer, J. J. Strouse, D. Kevelson, J. Phys. Chem. 100 (1996) 8518–8526.
- [4] P. F. McMillan, M. Wilson, D. Daisenberger, D. Machon, Nat. Mater. 4 (2005) 680–684.
- [5] Y. Katayama, K. Tsuji, J. Phys.: Condens. Matter 15 (2003) 6085–6103.
- [6] G. Monaco, S. Falconi, W. A. Crichton, M. Mezouar, Phys. Rev. Lett. 90 (2004) 255701.
- [7] W. Way, P. Wadhwa, R. Busch, Acta Mater. 55 (2007) 2977–2983.
- [8] H. W. Sheng, H. Z. Liu, Y. Q. Cheng, J. Wen, P. L. Lee, W. K. Luo, S. D. Shastri, E. Ma, Nat. Mater. 6 (2007) 192–197.

- [9] J. J. Z. Li, W. K. Rhim, C. P. Kim, K. Samwer, W. J. Johnson, Acta Mater. 59 (2011) 2166–2171.
- [10] Q. An, W. L. Johnson, K. Samwer, S. L. Corona, W. A. Goddard III, J. Phys. Chem. Lett. 11 (2020) 632–645.
- [11] Q. An, W. L. Johnson, K. Samwer, S. L. Corona, W. A. Goddard III, Acta Mater. 195 (2020), 274–281.
- [12] J. Shen, Z. Lu, J. Wang, S. Lan, F. Zhang, A. Hirata, M. Chen, X. Wang, P. Wen, Y. Sun, H. Bai, W. Wang, J. Phys. Chem. Lett. 11 (2020), 6718–6723.
- [13] J. Na, S. L. Corona, A. Hoff, W. L. Johnson, Proc. Natl. Acad. Sci. U. S. A. 117 (2020), 2779–2787.
- [14] S. Alexander, Phys. Rep 296 (1998), 65–236.
- [15] V. Vitek, T. Egami, Phys. Status Solidi B 144 (1987), 145–156.
- [16] V. A. Levashov, T. Egami, R. S. Aga, J. R. Morris, Phys. Rev. B 78 (2008), 064205.
- [17] J. D. Honeycutt, H. C. Andersen, J. Phys. Chem. 91 (1987) 4950–4963.
- [18] P. Steinhardt, D. Nelson, M. Ronchetti, Phys. Rev. B 28 (1983), 784–805.
- [19] W. Mickel, S. C. Kapfer, G. E. Schroeder-Turkand, K. Mecke, J. Chem. Phys. 138 (2013), 044501.
- [20] S. Plimpton, J. Comp. Phys. 117 (1995) 1–19.
- [21] P. L. Williams, Y. Mishin, J. C. Hamilton, Model. Simul. Mater, Sci. Eng. 14 (2006) 817–833.
- [22] M. H. Sadd, Elasticity Theory, Applications and Numerics, Elsevier, Oxford, U.K., 2009.
- [23] R. Hill, The Mathematical Theory of Plasticity, Clarendon Press, Oxford, U.K., 1950.
- [24] J. F. Lutsko, J. Appl. Phys. 65 (1989), 2991–2997.

- [25] P. A. Burrough, R. McDonnell, C. D. Lloyd, Principles of Geographical Information Systems, Oxford University Press, 2015.
- [26] Y. Le Page, P. Saxe, Phys. Rev. B 65 (2002) 104104.
- [27] D. Hull, D. J. Bacon, Introduction to Dislocations, 5th edition, Elsevier, 2011.
- [28] H. Tanaka, T. Kawasaki, H. Shintani, K. Watanabe, Nature Mater. 9 (2010), 324–331.
- [29] K. Lochmann, A. Anikeenko, A. Elsner, N. Medvedev, D. Stoyan, Eur. Phys. J. B 53 (2006), 67–76.

[30]

